AIAA Atmospheric Flight Mechanics Conference
13 - 16 August 2012, Minneapolis, Minnesota

AIAA 2012-4507

Atmospheric Data System Sensor Placement Optimization for Mars Entry, Descent, and Landing

Soumyo Dutta* and Robert D. Braun†
Georgia Institute of Technology, Atlanta, GA, 30332-1510, USA

and

Christopher D. Karlgaard‡
Analytical Mechanics Associates, Inc., Hampton, VA, 23666-1568, USA

The Mars Science Laboratory (MSL) contains an atmospheric data system that takes measurement of the pressure distribution on the entry body during the hypersonic and supersonic descent phases of the flight. This pressure data can be combined with other on-board sensors, such as accelerometers, gyros, and radar altimeter, to estimate the flight's trajectory, aerodynamics and the atmospheric profile. The number of sensors and their locations for the atmospheric data system can be optimized to increase the accuracy of the post-flight reconstruction. Methodologies based on using the estimation residual and a surrogate of the observability matrix are presented here and results of the optimization exercises for pressure transducer systems on Mars entry, descent, and landing (EDL) vehicles are shown. These techniques can be subsequently applied in the design of instrumentation suites of future EDL vehicles.

Nomenclature

A	Process eq. Jacobian (w.r.t. the state vector)
B	Process eq. Jacobian (w.r.t. the noise vector)
C	Surrogate of the innovation covariance matrix
H	Measurement sensitivity matrix
f	Function value
I	Identity matrix
J	Cost function
K	Kalman gain
m	Length of the Mach number vector
n	Number of pressure ports
P	State covariance
P	Pressure, Pa.
q	Dynamic pressure, Pa.
Q	State noise covariance
R	Measurement covariance
t	Time, sec
x	State vector
y	Measurement vector
α	Angle of attack, rad

*Graduate Research Assistant, Daniel Guggenheim School of Aerospace Engineering, AIAA Student Member.
†David & Andrew Lewis Professor of Space Technology, Daniel Guggenheim School of Aerospace Engineering, AIAA Fellow.
‡Senior Project Engineer, AIAA Senior Member.

β	Sideslip angle, rad

Subscript

0	Initial condition
i	State index
k	Time increment
obs	Observability matrix
∞	Freestream condition

Superscript

T	Transpose
$+$	Best estimate
$-$	Nominal estimate
$\widehat{\ }$	Estimated quantity

I. Introduction

The United States has successfully landed on Mars seven times since 1976. The entry vehicle for all of these missions was a 70-deg sphere cone aeroshell and the descent phase has used a supersonic parachute, although the final landing sequence has varied, with the Viking missions and Phoenix using a soft landing, Pathfinder and the Mars Exploration Rovers using an airbag system, and the Mars Science Laboratory using the sky-crane system.[1] Despite the similarity between the spacecraft, especially in the entry and descent phase of the vehicle trajectory, there still remain large uncertainties in the engineering models used during Mars EDL design and these uncertainties lead to design conservatism and a higher EDL system mass.

Flight data from EDL spacecraft can be used to reconstruct trajectory, atmosphere, and vehicle aerodynamic coefficients and thus allow for quantification of the uncertainties in the vehicle performance and the Martian environment. If statistical estimation methods are used for the reconstruction, then measurement noise and possible uncertainties in the dynamics of the state variables can be included in the estimation algorithm to improve both the state estimate and the uncertainty of the estimated state. The 2012 Mars Science Laboratory (MSL) mission contains a flush-mounted atmospheric data system (same as air data systems used for Earth applications) that takes measurement of the pressure distribution on the entry body during the hypersonic and supersonic descent phases of the flight.[2] This pressure data is collected by the Mars Entry Atmospheric Data System (MEADS) instrumentation, which is part of the larger Mars EDL Instrumentation (MEDLI) project. Together with the other on-board sensors, the pressure data can provide a good reconstruction of the flight's dynamic pressure, angle of attack, and sideslip angle without making any assumptions about the vehicle's aerodynamics and provides means of separating aerodynamic uncertainties from atmospheric uncertainties.[3,4]

The MEADS instrumentation suite was designed for the MSL trajectory[2,3] based on past Earth-based air data system designs and expert knowledge. However, there is a lack of work in the area of optimizing the locations of pressure transducers for an atmospheric data system. Since a MEADS-type system enables the separation of aerodynamic and atmospheric uncertainties, which are some of the most dominant uncertainties during EDL,[5] it is important to optimally place these instruments to enhance the reconstruction quality. An optimization exercise can also identify the minimum number of transducers needed to meet requirements for reconstruction. As future Mars missions test ambitious technologies, they are more likely to be instrumented with versatile atmospheric data system like sensors. These future atmospheric data systems on Mars EDL vehicles will need to be tailored for the trajectory of these vehicles and needs to be able reconstruct parameters of interest to within certain levels.

This study demonstrates a method to optimize the design of a future Mars EDL air data instrumentation suite so that EDL states, especially those that can help quantify atmospheric and aerodynamic uncertainties, can be accurately estimated. The optimization results are based on two types of objective function: (1) The residual between the estimated quantities and the truth data is shown in Sections III, IV, and V and (2) a surrogate of the observability matrix as shown in section VI.

II. Background

A. Mars Science Laboratory

MSL carries a set of instruments that take in-situ measurements of the pressure and temperature distribution on the aeroshell. The instrumentation is known as MEDLI and consists of MEADS to take the pressure measurements and Mars Integrated Sensor Plug (MISP) to take the aerothermodynamic data. Optimization of the location of MISP sensors is not covered by this current paper. MEADS's science objective is to reconstruct the atmospheric properties within certain bounds. Specifically when the dynamic pressure is greater than 850 Pa., the objective is to estimate freestream Mach number (M_∞) to within ± 0.1, dynamic pressure (q_∞) to within $\pm 2\%$, and angle of attack (α) and sideslip angle (β) to within ± 0.5 deg.[2] In order to achieve these targets, MEADS collects pressure data from seven pressure transducers located around the forebody of the aeroshell (see Figure 1).

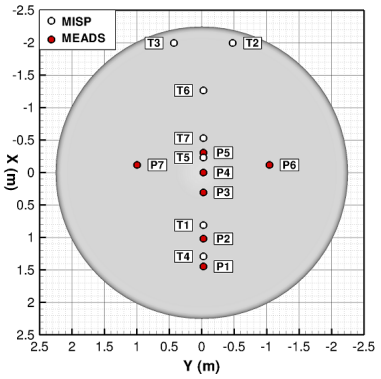

(a) MEDLI instrument locations[6]

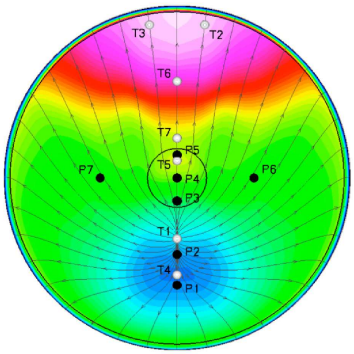

(b) Expected qualitative heating rate which demonstrates the location of the stagnation region in blue.[2]

Figure 1. MEDLI sensor locations. P signifies pressure transducers and T marks the locations of the thermocouple plugs.

The locations of the transducers are based on the predicted pressure distribution on the aeroshell; however, no quantitative optimization procedure was conducted in the selection of the transducer locations. It is expected from the nominal trajectory that the stagnation pressure is to be around transducers P1 and P2, while P6 and P7 serve as the transducers that will help reconstruct the sideslip angle. All of the transducers besides P6 and P7 are expected to help reconstruct the angle of attack history. Although the transducers that are used for MEADS can sample at high rates, due to memory constraints, both pressure and temperature data will be saved at an effective sampling rate of 8 Hz.[2]

B. Past Use of Atmospheric Data Systems

Vikings 1 and 2 were the first Martian spacecraft with flush atmospheric data systems; however, the data from these spacecraft had significant noise and was in general unintelligible.[7] Other reentry vehicles have utilized atmospheric data systems. Flight reconstructions of these EDL vehicles have generally utilized pressure data in conjunction with statistical estimation procedures to estimate trajectory, atmosphere, aerodynamics, and the associated uncertainties. One of the most famous examples is the Shuttle Entry Air Data System (SEADS) program of the 1980's that used a flush-mounted air data system on the shuttle's nose to estimate the pressure distribution across the space shuttle forebody during entry.[8,9] The MEDLI program's pressure data system is in large part based on the SEADS concept.[2] The SEADS project was able reconstruct the freestream conditions during shuttle entry successfully and verified its results with simulation and wind tunnel data.[10,11] However, reconstructions based on SEADS data did not blend the inertial measurements with the pressure distribution data. Instead, a sequential filter was used in conjunction with a database of pressure distributions on the vehicle forebody to inversely estimate the aerodynamic parameters that could create the pressure measurements at the transducers.[9,10] Thus, potential coupling between trajectory and atmospheric uncertainties were not considered by that analysis.

Flush air data systems have also been used for high angle of attack aerodynamic research,[12,13] hypersonic

experiments,[14] and for conceptual studies for munition guidance.[15,16] Some of the reconstruction techniques have also used statistical estimators to reconstruct atmosphere and trajectory simultaneously,[17] thus preserving the coupling in the estimation algorithm between these two types of parameters. However, similar to SEADS, these applications did not use any physics-based optimizing routine to select the transducer locations.

C. Optimization of Atmospheric Data Systems

As mentioned earlier, there has been limited work in the past to optimize the design atmospheric data systems in EDL vehicles. One of the few optimization studies for air data systems was conducted in the early 1990's in support of the Pressure Distribution/Air Data System (PD/ADS) experiment that was proposed to be included in the Aeroassist Flight Experiment (AFE), which was later canceled. In the study, Deshpande et al.[18] used a gradient-based estimator and a genetic algorithm (GA) to optimize the distribution of the PD/ADS sensors in order to decrease the effect of normally distributed random noise of the pressure transducers. The work by Deshpande et al. used modified Newtonian theory for the predicted pressure model and a batch-type reconstruction process to estimate air data parameters, such as dynamic pressure, angle of attack, and sideslip angle. The residuals between the estimated parameters and their known, true values were then used in a single-objective function for the optimization routines.

An important difference between the work in this paper and Deshpande et al.'s work is that the previous study only considered reconstruction of a single trajectory point (one Mach number, dynamic pressure, etc.). Such a situation can be imagined for a wind tunnel testing, where pressure transducers on a test object's forebody collect data while the object is kept at the same flow conditions for a fixed period of time. So the reconstruction process (which serves as the objective function for the optimization problem) is expected to converge to a single trajectory state, unlike the case of EDL reconstruction where the trajectory states keep changing. Optimization of sensor locations where the signal will change with time has not been conducted previously for atmospheric data systems to the authors' knowledge.

Additionally, the EDL reconstruction process shown in this paper uses a pressure distribution prediction model based on the aerodynamic database of the vehicle. This database incorporates data from higher fidelity models based on Computational Fluid Dynamics (CFD) and wind tunnel data and is expected to be more accurate than the modified Newtonian assumption used by Deshpande et al.

D. Sensor Placement Problem as Multi-objective Optimization

The air data optimization study by Deshpande et al. turned a multi-objective optimization problem (optimizing the reconstruction of dynamic pressure, angle of attack, and sideslip angle) into a single-objective optimization problem. That study also used weighting parameters in order to turn the multiple objectives into a single objective and thus introduced some subjectivity into the optimization process.

However, since that study, the field of multi-objective optimization has matured, and the concept of Pareto dominance can be coupled with different types of optimization techniques to enhance several objective functions concurrently without the necessity of weighting functions.[19] The Pareto dominance concept is especially useful for evolutionary algorithms, such as GA, which can solve multi-modal problems better than traditional gradient-based methods, which often get stuck in local minima. In fact, outside the area of atmospheric data system, studies have been conducted that have found optimal locations for sensor and actuator placement using multi-objective optimization.[20] Many of these studies have utilized evolutionary algorithms, like GA and Particle Swarm Optimization (PSO), in order to find these optimal locations and can be found in Ref.[20]

Since the sensor placement problem for atmospheric data system has many, non-unique solutions, it is expected to be multi-modal and can benefit from such a procedure. In this paper, the concept of Pareto dominance, evolutionary algorithms which can handle multi-objective optimization, and the EDL reconstruction process are combined to demonstrate a methodology to optimize atmospheric data systems similar to the MEADS instrument of MSL. Such a procedure can advance the work by Deshpande et al. and allow future designers to determine the optimal number and locations of sensors on vehicles and objects that use atmospheric data systems for measurement.

III. EDL Reconstruction

The statistical reconstruction procedure is a key element in the optimization procedure, since the residual of the truth from the estimated parameters helps calculate the objective function for the optimizing method. The methodology used for reconstructing Mars EDL vehicle flight parameters involves taking EDL sensor measurements and using an estimation procedure to reconstruct the vehicle trajectory and atmospheric profile (see Figure 2). The estimated trajectory and atmospheric parameters can then be used to calculate the aerodynamic coefficients.

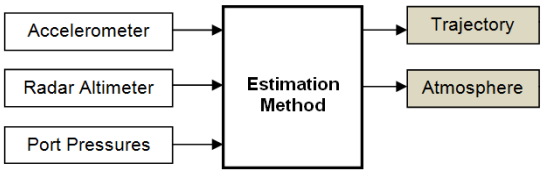

Figure 2. EDL reconstruction methodology.

For this paper, an extended Kalman filter (EKF) was used as the statistical estimator. The estimation process is summarized in Figure 3. The algorithm is presented in the next section.

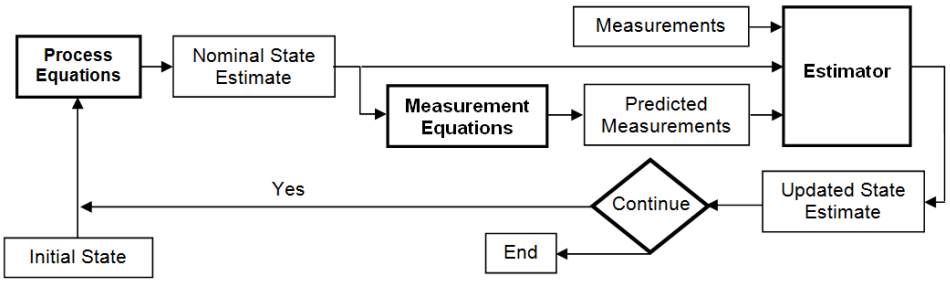

Figure 3. EKF reconstruction flow diagram.

A. Extended Kalman Filter

Extended Kalman filters have been extensively used in the past for Mars EDL reconstruction.[3,21–25] The algorithm for this well-known filter is summarized below:[26,27]

1. Initialize the state vector and the state covariance matrix at time $t_{k-1} = t_0$ and let $k = 1$, where k is an index of the epoch when a measurement is first available.
2. Read in the measurement at time t_k.
3. Calculate a nominal state ($\hat{x}_k^-$) at time t_k by integrating the non-linear equations of motions with $\hat{x}_{k-1}^+$ as the initial condition.
4. Calculate the nominal state covariance matrix ($\hat{P}_k^-$) by integrating the Riccati equations (Eq. (1a)).
5. Calculate the measurement residual vector (y_k), the measurement sensitivity matrix (H_k), and the Kalman gain (K_k) using the nominal state and state covariance (Eq. (1b)).
6. Calculate the best estimate of the state ($\hat{x}_k^+$) and state covariance ($\hat{P}_k^+$) using Eqs. (1c) and (1d).
7. Increment counter k and go back to step 2 until measurements at all times have been processed.

$$\dot{P} = AP + P^T A^T + BQB^T \tag{1a}$$

$$K_k = \hat{P}_k^- H_k^T \left(H_k \hat{P}_k^- H_k^T + R_k \right)^{-1} \tag{1b}$$

$$\hat{x}_k^+ = \hat{x}_k^- + K_k \left(y_k - h\left(\hat{x}_k^- \right) \right) \tag{1c}$$

$$\hat{P}_k^+ = (I - K_k H_K) \hat{P}_k^- (I - K_k H_k)^T + K_k R_k K_k^T \tag{1d}$$

The measurement covariance matrix (R) is defined at time k and information from sensor calibration is used in this matrix. The covariance of the state noise vector (Q) consists of noise variables in the process equations, such as the sensor uncertainty of the angular rate gyroscopes or tuning parameters for the velocity vector equations. See Ref. 4 for more information about state and measurement noise vectors and covariances. A is the Jacobian of the process equations with respect to the state vector, while B is the Jacobian of the process equations with respect to the state noise vector. The state noise vector for EDL reconstruction comes from uncertainties in the process equations, such as aerodynamic and atmospheric uncertainties. The matrix I in the covariance update equation is the identity matrix.

B. Process and Measurement Equations

As shown in Figure 3, the reconstruction process revolves around using process equations and measurement equations to inversely reconstruct trajectory and atmospheric states from sensor data. The process equations describe the dynamics of the estimation states, and since this is a trajectory and atmospheric reconstruction process, the process equations are equations of motion (EOM). The specific EOMs used here are based on translational equations derived in Ref. 28 with the addition of rotational dynamics and dynamic equations for freestream pressure and density. The complete set of EOMs can be found in Ref. 4. Discussion about the development of the dynamic equations for freestream pressure and density as well as assumptions made can be found in Refs. 3, 4, and 29.

The sensors used for the reconstruction process consist of IMU data, which includes accelerometers and gyro rates, radar altimeter, and of course the MEADS pressure data. Gyro rates are used in the process equations (as discussed in Ref. 4) and thus no measurement equations are needed for it. However, the other three data types need some form of equation where the estimation state vector could be used to predict measurement values. The measurement equation and the measurement sensitivity matrix for accelerometer data can be found in Refs. 23 and 30. Refs 23 also gives similar measurement equations for the radar altimeter. The measurement equation for the MEADS data consists of using the best estimated angle of attack, sideslip angle, dynamic pressure, and Mach number, the locations of the ports, and a CFD-derived pressure look-up table to predict the measured pressure at each port. Refs. 3 and 29 discuss this procedure and Ref. 29 also shows a example of the pressure look-up table.

C. Simulated Trajectory

The Mars EDL data is simulated in this study to demonstrate the effectiveness of the statistical reconstruction methodology that can incorporate disparate data types and estimate trajectory, atmospheric parameters and aerodynamic coefficients. The Program to Optimize Simulated Trajectories II (POST2)[31] was used to generate a nominal MSL-like trajectory that is presented in Figure 4. The trajectory is for a 4.5 m 70-deg sphere-cone with the same geometry and specifications as MSL. This trajectory represents the truth data and the reconstructed values are compared with it.

The POST2 outputs are used to generate Inertial Measurement Unit (IMU) data, radar altimeter measurements (when the altitude is less than 10 km), and MEADS-type data (when the dynamic pressure is greater than 850 Pa.) using the same measurement equations that are used in the estimator but with random noise added to the measurements. The 850 Pa. limit mimics the time frame in which the actual MEADS is going to take its data.[2] Future instrumentation with more sensitive sensors may not be limited to this range and vehicle trajectories might allow the atmospheric data system to take measurement beyond simply the supersonic phase of the flight. However, for this study, this restriction was maintained. The plots for angle of attack, sideslip angle, and dynamic pressure are limited to a time window of 0 to 200 seconds since the MEDLI system roughly operates in this time period. Refer to Ref. 4 for information regarding the noise added to the dataset.

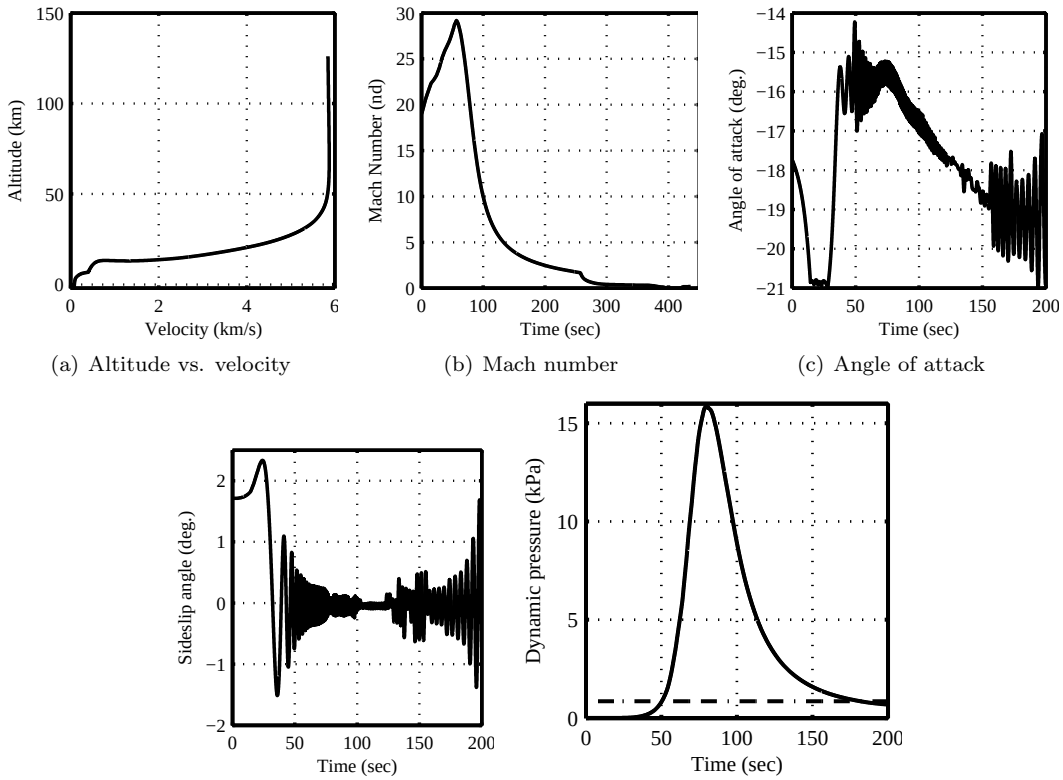

(a) Altitude vs. velocity (b) Mach number (c) Angle of attack

(d) Sideslip angle (e) Dynamic pressure (solid), 850 Pa. (dashed)

Figure 4. Simulated trajectory used for creating the dataset.

D. Sample Reconstruction Results

Sample results from the EDL reconstruction methodology are shown in Figure 5. The reconstructed parameters shown are the best estimated angle of attack, sideslip angle, and dynamic pressure. These three states are parameters of interest for the MEADS science objectives and the residual between the best estimated values and the actual values of these parameters can serve as an objective function with which to optimize the air data sensor locations. The results shown in Figure 5 are for the time frame when dynamic pressure is greater than 850 Pa., but the reconstruction occurs from atmospheric interface to touchdown.

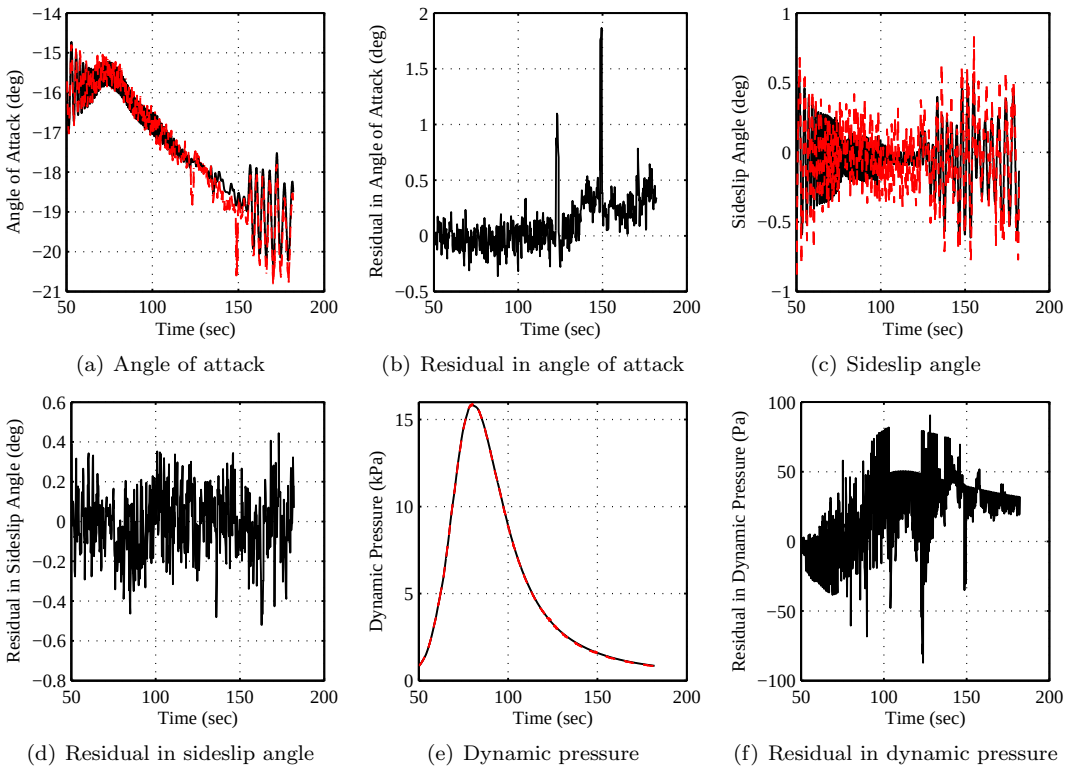

(a) Angle of attack (b) Residual in angle of attack (c) Sideslip angle

(d) Residual in sideslip angle (e) Dynamic pressure (f) Residual in dynamic pressure

Figure 5. Example of results from the EDL reconstruction process. Actual trajectory (solid, black), best estimate (dashed, red).

IV. Optimization Method

The previous section described the EDL reconstruction procedure which provides the quantitative information for the optimization algorithm. This section describes this optimization algorithm in more detail and presents the objective function used to optimize the placement of the atmospheric data system sensors.

Since multi-objective optimization procedures are used, the problem involves finding solutions that represent tradeoffs among conflicting objective functions. The set of all of these solutions represent non-dominated solutions in the design space, and the set of non-dominated solutions are referred as a *Pareto frontier*. The concept of *domination* states that a point x_1 dominates another point x_2 if the objective function vector f of x_1 is no worse than the objective function vector of x_2 and the function value x_1 is strictly better that the function value of x_2 along at least one dimension of the objective function.[19] All of the points that are not dominated by any other point in the design space are members of the Pareto front. The optimization routine used here is a variant of the Genetic Algorithm. As mentioned earlier, these techniques are beneficial in function spaces that are multi-modal and these algorithms can also find many points of the Pareto frontier simultaneously instead of finding one point of the Pareto frontier at a time like traditional optimization techniques.

A. Cost Function

The main objective in optimizing the layout of the pressure port system is to enhance the accuracy of the reconstruction process. Since the EKF is being used as the statistical estimator, then the reconstructed parameters are theoretically supposed to be good estimates of the true states based on the dataset that is available. So the goal of the layout optimizing exercise is to choose the number of transducers and the locations of the sensors so that the measurements themselves would be the *optimal dataset* to reconstruct the flight parameters of interest.

For the MEADS project, the main parameters of interest are the dynamic pressure, angle of attack, and sideslip angle. So the cost function (J) is represented by the residual between the estimated flight parameters and their true values. This is similar to what Deshpande et al.[18] used for the PD/ADS optimization; however,

the past study used some form of a weighting factor to choose which parameter of interest is more valuable, which adds some subjectivity to the optimization exercise. More importantly, the parameters being estimated were static and not changing with time, unlike the case for the trajectory reconstruction of a Mars EDL vehicle. For this exercise, the cost functions for each parameter are combined into a vector that will be optimized using Pareto dominance.

The residuals of the parameters are calculated at certain Mach numbers along the trajectory and the maximum residual is reported as the objective function value. The residuals are also normalized by the MEADS science objective value, i.e. 2% for q_∞ and 0.5 deg for α and β. Thus, an objective function value between 0 and 1 signifies that the port combinations produce data that can be reconstructed by the EKF to within MEDLI science objectives. The cost function is stated in Eqs. (2), where i is an index for the m-length Mach number vector over which the residuals are calculated. For this objective function $M_{\infty,i} = [14, 16, 18, 20, 24]$, which all fall within the timeframe the MEADS instrument operates.

$$\min J = \min \left[J_\alpha, \quad J_\beta, \quad J_{q_\infty} \right] \tag{2a}$$

$$J_\alpha = \max_{i=1}^{m} \left| \frac{\alpha_{\text{recon},i} - \alpha_{\text{true},i}}{\alpha_{\text{MEDLI objective}}} \right| \tag{2b}$$

$$J_\beta = \max_{i=1}^{m} \left| \frac{\beta_{\text{recon},i} - \beta_{\text{true},i}}{\beta_{\text{MEDLI objective}}} \right| \tag{2c}$$

$$J_{q_\infty} = \max_{i=1}^{m} \left| \frac{\left(q_{\infty,\text{recon},i} - q_{\infty,\text{true},i}\right) / q_{\infty,\text{true},i}}{q_{\infty,\text{MEDLI objective}}} \right| \tag{2d}$$

Additionally, some geometric constraints were added to the problem. The port locations were restricted to within a 2 m radius on the forebody (to restrict sensors on the vehicle shoulder) and the ports had to be at least 0.125 m ($\approx$ 5 inches) apart.

The objective function in this section is not unique for the air data sensor optimization procedure; in fact, later in this paper, another optimization procedure is discussed that is faster than the procedure from this section. Thus, it should be emphasized that this procedure is merely the first attempt at sensor optimization and more work needs to be done to improve this methodology while characterizing the most appropriate objective function.

B. NSGA-II

The optimization technique used for this exercise is the Non-dominated Sorting Genetic Algorithm II (NSGA-II).[19,32] This optimization technique has been used extensively to solve many multi-objective optimization problems and is considered a baseline technique in the field.[33]

The optimization algorithm consists of three basic steps: initialization, sorting, and reproduction (see Fig. 6). The optimizer initiates a randomly generated population of feasible port locations and then assigns them into different fronts based on the objective function values. Also, the crowding distance in the objective function space between different design parameters is also calculated. In successive iterations (or generations), the optimizer uses an elitist technique to pair the most Pareto dominant parents to produce children using tournament selection, crossover, and mutation operations and the process is repeated for a user-defined period of time. It is expected that the final generation will be close to the theoretical Pareto frontier.[32]

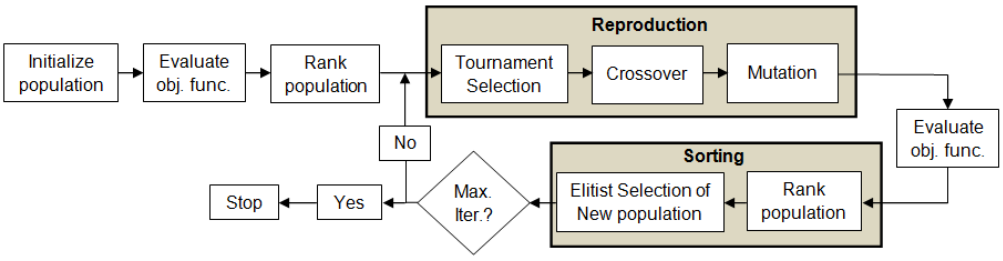

Figure 6. Flow diagram of NSGA-II.

The algorithm handles constraints during the tournament selection process. The rule, in order, is to

select the best solution among two feasible solutions, choose the feasible solution, or to choose the solution with the smallest constraint violation.[19] The optimization routine was programmed in MATLAB®.[34]

V. Results

The main objective of the optimization methodology is to identify (1) minimum number of ports needed for accurate reconstruction and (2) the optimal location of the ports for each configuration. As two of the parameters of interest are orientation angles, the minimum number of ports studied are the two port configurations, since angular value estimation requires at least two points of reference. For consistency with the MEADS configuration, seven ports serves as the upper bound.

The study is broken into three steps. First, single-objective optimization is performed to identify the best configurations for systems for a given objective function and number of ports. Next, two-objective optimization is performed on each pair of objective functions to study the tradeoffs in the design space and visualize the Pareto frontier environment. Finally, all three objective functions are simultaneously optimized.

A. Single-objective Optimization

The optimizer is used to find optimal configurations that minimize each objective functions for two, three, four, five, six, and seven port configurations. Convergence to the global minima cannot be guaranteed due to the stochastic nature of the optimizer; thus, each optimization is repeated at least 10 times using different random number seeds. Also, each optimization run is continued for at least 100 generations, as it was found that the minimization routine converged to the lowest possible function values by at least the 100th iteration. The maximum population size was limited to 32 members to limit number of function calls per generation; however, smaller population size leads to the Pareto frontiers that maybe sparse. Thus, future work will rectify this by increasing the population size.

Figure 7 shows the minimum objective function value found using single-objective optimization for a specific number of ports. Additionally, Table 1 summarizes the objective function vector for each of the single-objective optimization points noted in Fig. 7. Recall that the objective function values were normalized so that values between 0 and 1 signify that a configuration meets the minimum MEDLI objectives. One sees that the optimal configuration for one objective function value often leads to unacceptable levels in the other objective functions. As a baseline, reconstruction of the simulated dataset using the MEADS configuration yielded $[J_\alpha, \quad J_\beta, \quad J_{q,\infty}] \quad = \quad [0.1657, \quad 0.0321, \quad 0.7876]$.

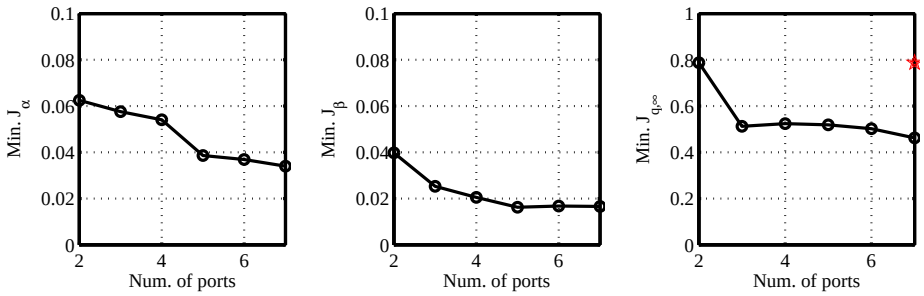

(a) α (b) β (c) q_∞

Figure 7. Results of single-objective optimization. MEADS (red star) in q_∞ plot.

Table 1. Objective function vectors for the results of single-objective optimization.

Num. ports	2	3	4	5	6	7
			Min. J_α			
J_α	0.06246	0.05757	0.05408	0.03862	0.03687	0.03397
J_β	2.217	0.4953	0.24531	0.0486	0.052595	0.06094
$J_{q\infty}$	1.033	1.0413	0.75394	1.059	1.102	1.0787
			Min. J_β			
J_α	6.366	2.932	0.6574	0.1629	0.18525	0.1389
J_β	0.03976	0.02527	0.02052	0.01624	0.01673	0.01659
$J_{q\infty}$	1.155	1.176	1.0378	1.0558	0.9786	0.6746
			Min. $J_{q\infty}$			
J_α	0.83212	0.1032	0.1072	0.1256	0.09104	0.082205
J_β	1.701	0.57362	0.096619	0.083149	0.072913	0.04621
$J_{q\infty}$	0.7877	0.5123	0.5237	0.5187	0.5023	0.4621

Figure 8 shows the optimum configuration for some of the single-objective results. The minimum dynamic pressure (Fig. 8(a)) result shows that the optimum configuration is to place the two ports in the stagnation region, similar to what MEADS has done. Of course, the improvement in the pressure estimation comes at the cost of worse sideslip angle and angle of attack detection. The minimum sideslip angle solution (Fig. 8(b)) spreads the four ports across the horizontal axis, but the ability to reconstruct dynamic pressure and angle of attack deteriorates. The seven port minimum angle of attack result (Fig. 8(c)) is interesting as the configuration puts the pressure transducers on the spherical nose cap making the configuration sensitive to changes in the angle of attack, but also worsening the dynamic pressure reconstruction ability. Surprisingly, since the ports are spread around the spherical nose cap, there is some sideslip angle resolution. It is likely that the optimizer was trying to co-locate some of the sensors at the same spots but was prevented by the minimum distance between sensors constraint.

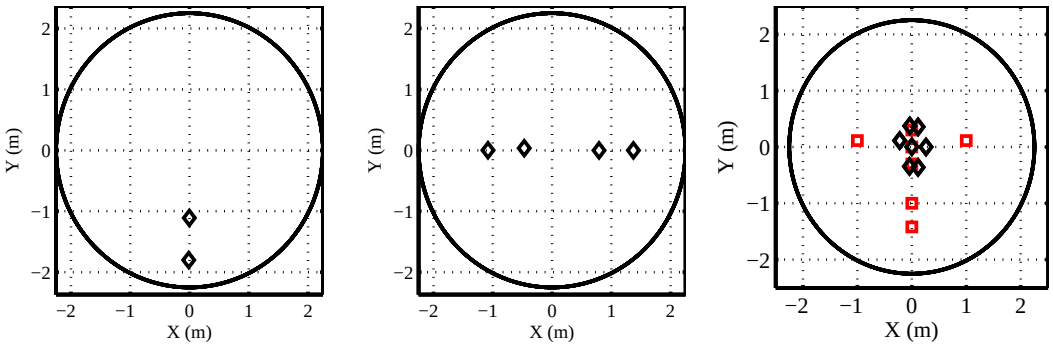

(a) Two port min. $J_{q\infty}$ (b) Four port min. J_β (c) Seven port min. J_α, MEADS (red square)

Figure 8. Some representative configurations from single-objective optimization results.

B. Two-objective Optimization

The results of the single-objective optimization showed that configurations that maximized the reconstruction capability of one parameter penalized the estimation of the other parameters. These tradeoffs are visualized using Pareto fronts developed from the results of two-objective optimization as seen in Fig. 9. Zoomed insets of each pair of two-objective optimization are also provided.

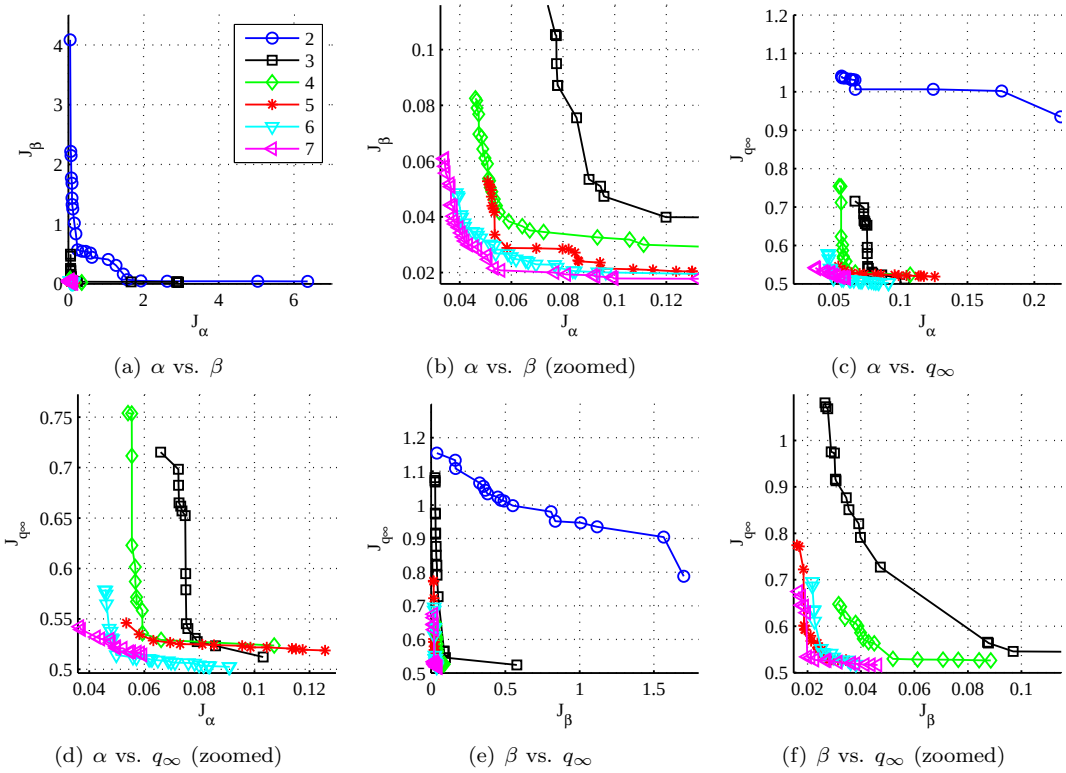

(a) α vs. β (b) α vs. β (zoomed) (c) α vs. q_∞

(d) α vs. q_∞ (zoomed) (e) β vs. q_∞ (f) β vs. q_∞ (zoomed)

Figure 9. Results of two-objective optimization.

It should be emphasized that although the Pareto frontiers of cases with different number of ports are plotted together in Fig. 9, in reality each Pareto frontier is a solution to a separate optimization problem with a separate design space. For example, there is no relation between the $J_\alpha - J_\beta$ Pareto frontier for the two port case and the three port case. One expects that as the number of ports increase the overall objective function values will decrease, but it is not as if the three port case builds on the result of the two port Pareto frontier case. Each optimization scenario is randomly initialized and the optimization procedures for different number of port cases do not share information with each other.

The Pareto frontiers in Fig. 9 do coalesce onto each other as the number of ports increase. This behavior signals a diminishing return type of behavior when the number of ports are increased. Upon inspection of the inset figures, it appears that when looking at α and β reconstruction performance, the six and the seven port results are close to each other. There is little gained in adding an additional port to go from six to seven ports for this trade. Looking at the other two trades, the five port solution appears to match the six and seven port results in the β and q_∞ trade but remains far off from the six and seven port results in the α and q_∞ trade. The diminishing return thus appears to be close to the six port Pareto front. Recall that the MEADS configuration yields $[J_\alpha, \quad J_\beta, \quad J_{q,\infty}] \quad = \quad [0.1657, \quad 0.0321, \quad 0.7876]$, which puts that configuration in the dominated solution space of the seven port Pareto frontiers, albeit not too far off the front. Of course, it should be stressed that this observation is for the current objective function only, and other formulations of the cost function might improve the ranking of the MEADS configuration.

C. Three-objective Optimization

For the final optimization case, all three objective functions were minimized simultaneously by the NSGA-II optimizer. Figure 10 shows the optimization's results for the various number of port cases. Additionally, the MEADS baseline is also shown on the seven port plot for comparison, even though it is not a Pareto-optimal solution according to the optimization.

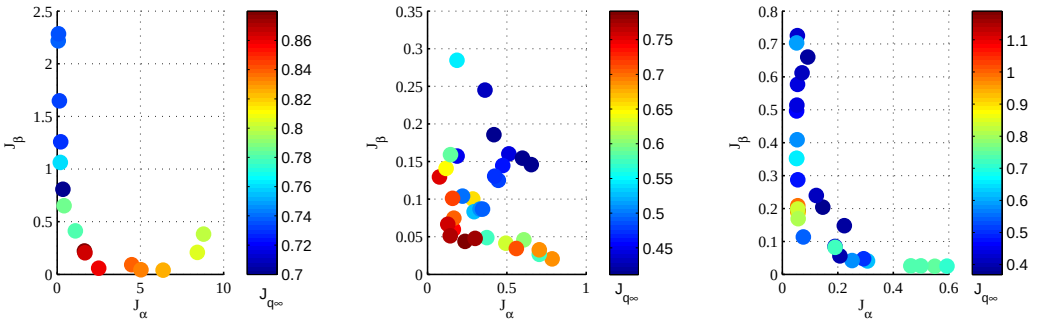

(a) Two port (b) Three port (c) Four port

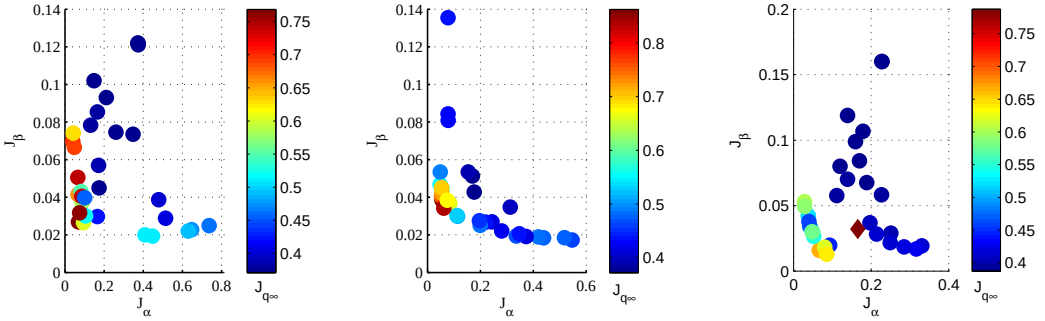

(d) Five port (e) Six port (f) Seven port, MEADS (diamond)

Figure 10. Results of three-objective optimization.

Some representative seven port cases from the Pareto-optimal solutions are shown in Fig. 11 and their objective function value is compared to the MEADS configuration in Table 2. The first case shows a configuration that improves the angle of attack and sideslip angle capabilities from MEADS, but is worse off in estimating the dynamic pressure. The second figure is the opposite case, as dynamic pressure reconstruction ability improves due to extra ports near the stagnation point, but decreases angle of attack and sideslip angle estimation ability. Through an optimization exercise such as the one conducted in this paper, an atmospheric data system designer can decide which way he wants to move in the design space.

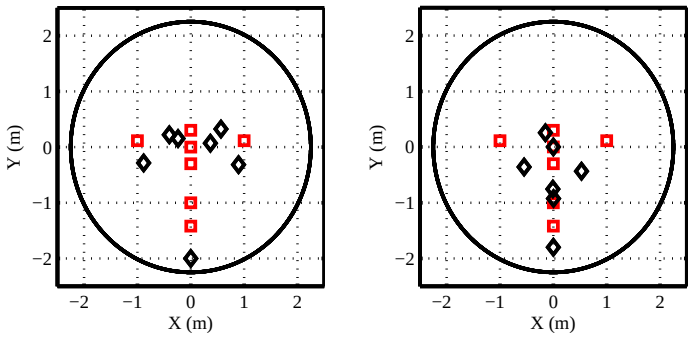

(a) Case 1: Lower J_α and J_β (b) Case 2: Lower $J_{q\infty}$

Figure 11. Some representative configurations from three-objective optimization results. MEADS (red square), optimized (black diamond)

Table 2. Comparison of seven port representative cases with the MEADS configuration.

	Case 1		Case 2	
	Value	% Diff. MEADS	Value	% Diff. MEADS
J_α	0.06608	-60%	0.22787	+38%
J_β	0.015924	-50%	0.16001	+398%
$J_{q\infty}$	0.934463	+19%	0.541879	-31%

VI. Observability-based Objective Function

The objective functions used so far in this paper and in the work of Deshpande et al.[18] have used the residual between the reconstructed parameters and the truth to drive the optimization process. However, since the objective function consists of an inverse estimation procedure, the function could be defined in a way to maximize the *observability* of the dataset. Observability, in estimation theory is the concept of how well the state vector (parameters of interest) can be deduced from the outputs.[26] Observability matrices are hard to calculate for non-linear, time varying system, but the measurement sensitivity matrix, H, seen previously in the algorithm for the EKF, serves as a good surrogate. The measurement sensitivity matrix is the Jacobian matrix of the measurement with respect to change in the state vector. The state vector of interest for the MEADS case is of course $x = [\alpha, \beta, q_\infty]^T$ and the measurement is the n-number of ports pressure data. The objective function J could then be defined as shown in Eqs. 3 where the J_{obs} is to be minimized. The 3×3 matrix C is a surrogate of the innovation covariance matrix that is seen in Least-Squares estimators and in the Kalman gain (see Eq. 1b) and gives a metric for estimating the observability matrix. The same geometric constraints as before (2 m radius limit and 0.125 m minimum distance between ports) are also applied.

$$H = \frac{\partial \mathrm{P}_i}{\partial x} \quad i = 1, ..., n \tag{3a}$$

$$C = \left(HH^T\right)^{-1} \tag{3b}$$

$$J_{\text{obs}} = \frac{C_{1,1}}{\alpha^2_{\text{MEDLI objective}}} + \frac{C_{2,2}}{\beta^2_{\text{MEDLI objective}}} + \frac{C_{3,3}}{q^2_{\infty,\text{MEDLI objective}}} \tag{3c}$$

The objective function above was tested at various MSL, flight-relevant conditions as summarized in Table 3. A baseline case of the 7-port MEADS sensors is given as an initial condition and then a MATLAB®[34] provided Sequential Quadratic Programming tool is used to solve the minimization problem. Since a gradient-based optimization procedure is being used, it is possible that the optimization procedure can be stuck at local minima. Further study will involve using this procedure with the NSGA-II algorithm. Although this procedure does not give Pareto frontiers of possible port locations, the optimization is quick. Each function call in this case takes 10^{-3} seconds, while the optimization procedure involving a entire trajectory reconstruction and then computing the residual between estimated and true values needed 25 seconds per run as written in MATLAB. Hence, a non-residual objective function like J_{obs} offers an advantage in computation speed.

Table 3. Flight-relevant test conditions for J_{obs}.

Case No.	1	2	3	4	5	6	7	8	9
M_∞	28	28	28	19	19	19	8	8	8
q_∞ (Pa.)	850	850	850	16000	16000	16000	6000	6000	6000
α (deg.)	-24	-20	-16	-24	-20	-16	-24	-20	-16
β (deg.)	0	0	2	0	0	0	1	0	0

Figure 12 shows the results of the optimization procedure. Since a gradient-based optimization procedure is used, the optimized values stay around the same basin of attraction as the initial guess. However, it is interesting to note that when β values are non-zero, the optimized configuration deviates significantly from

the MEADS configuration as seen in the figure for case 3. These deviations underscore the need to conduct physics-based optimization exercises to optimally place atmospheric data system sensors. The MEADS configuration seems to work well for situations with $\beta = 0$ deg. and high M_∞, but any deviation from those conditions, which is expected in a time-varying trajectory, leads to off-optimal behavior from the MEADS configuration.

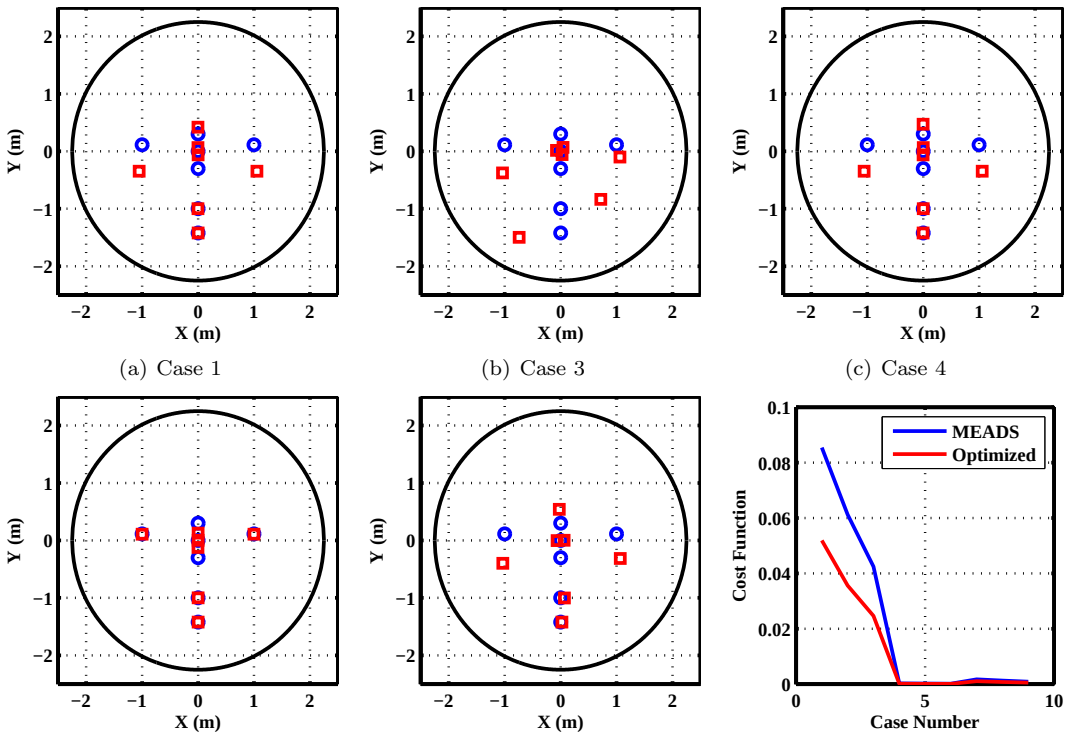

(a) Case 1 (b) Case 3 (c) Case 4

(d) Case 6 (e) Case 7 (f) Objective function values

Figure 12. Results of observability matrix based optimization for seven port configuration. MEADS (blue circle), Optimized (red square).

VII. Conclusion

Mars EDL design contains large uncertainties in the knowledge of atmospheric properties and aerodynamic coefficients of the vehicles. A major element of the difficulty has been that past EDL flight datasets have not allowed atmospheric and aerodynamic parameters to be independently observable. The MSL dataset includes pressure data from an on-board atmospheric data system that can allow separation of aerodynamic and atmospheric uncertainties; however, the design of the atmospheric data system was not optimized using a physics-based optimization routine. In fact, there is little work in the literature regarding optimization of sensor placements for atmospheric data systems.

This paper introduces two possible optimization methodologies that could help designers plan the quantity and the locations of pressure transducers to reconstruct EDL flight parameters of interest such as angle of attack, sideslip angle, and dynamic pressure. The first method presented uses the residual between the best estimated trajectory from a given dataset and the true parameter values to optimize the location of the ports. Since the design space is multi-modal and multi-objective, an evolutionary algorithm that can handle multiple objective functions has been used to show results for single-objective, two-objective, and three-objective optimization results. These procedures give representative port configurations that can improve reconstruction performance from the MEADS baseline. Additionally, an observability matrix based optimization method is also presented to allow design space exploration in a computationally faster way.

This paper advances the state-of-the-art in sensor placement problem, specifically for atmospheric data system optimization, and introduces residual and non-residual based optimization methodologies that can be beneficial to the designer of future Mars EDL atmospheric data systems. The methodology of this paper can

be used to find the design parameters that provide the optimized configuration of atmospheric data sensors without assuming *a priori* any weighting function or subjective criterion. Any subjective weighting criteria can be applied during post-processing of the data without having to re-run the optimization procedure. The optimization technique shown here together with the Pareto dominance concept allows a designer to locate most of the best configurations in a short period of time and thus allows for the optimal placement of sensors hitherto rarely discussed in the field of atmospheric data systems.

Acknowledgments

A NASA Research Announcement (NRA) award (No. NNX12AF94A) has supported some of the tool development effort. The authors want to thank the grant's point of contact, Bernie Laub of NASA Ames Research Center, for his support for the research, and Scott Striepe, of NASA Langley Research Center, for his advice and help in acquiring the simulated datasets and other related tools. The authors are grateful to Mark Schoenenberger of NASA Langley Research Center for providing data for the analysis and advice regarding the analysis. Also, the authors would like to thank Milad Mahzari at Georgia Tech for his help in editing the paper.

References

[1]Braun, R. D. and Manning, R. M., "Mars Exploration Entry, Descent, and Landing Challenges," *Journal of Spacecraft and Rockets*, Vol. 44, No. 2, 2007, pp. 310–323.

[2]Gazarik, M. J., Wright, M. J., Little, A., Cheatwood, F. M., Herath, J. A., Munk, M. M., Novak, F. J., and Martinez, E. R., "Overview of the MEDLI Project," *IEEE Aerospace Conference*, IEEE, March 2008.

[3]Karlgaard, C. D., Beck, R. E., Keefe, S. A., Siemers, P. M., White, B. A., Engelund, W. C., and Munk, M. M., "Mars Entry Atmospheric Data System Modeling and Algorithm Development," *AIAA Thermophysics Conference, San Antonio, TX*, No. AIAA 2009-3916, 2009.

[4]Dutta, S., Braun, R. D., Russell, R. P., Clark, I. G., and Striepe, S. A., "Comparison of Statistical Estimation Techniques for Mars Entry, Descent, and Landing Reconstruction from MEDLI- like Data Sources," *AIAA Aerospace Sciences Meeting, Nashville, TN*, No. AIAA 2012-0400, 2012.

[5]Striepe, S., Way, D., Dwyer, a. M., and Balaram, J., "Mars Science Laboratory Simulations for Entry, Descent, and Landing," *Journal of Spacecraft and Rockets*, Vol. 43, No. 2, March 2006, pp. 311–323.

[6]Edquist, K. T., Dyakonov, A. A., Wright, M. J., and Tang, C. Y., "Aerothermodynamic Design of the Mars Science Laboratory Heatshield," *AIAA Thermophysics Conference, San Antonio, TX*, No. AIAA 2009-4075, 2009.

[7]Ingoldby, R., Michel, F., Flaherty, T., Doty, M., Preston, B., Villyard, K., and Steele, R., "Entry Data Analysis for Viking Landes 1 and 2," Tech. Rep. NASA CR 159388, National Aeronautics and Space Administration, 1976.

[8]Siemers, P. M. and Larson, T. J., "Space Shuttle Orbiter and Aerodynamic Testing," *Journal of Spacecraft*, Vol. 16, No. 4, 1979, pp. 223–231.

[9]Pruett, C. D., Wolf, H., Heck, M. L., and Siemers, P. M., "Innovative Air Data System for the Space Shuttle Orbiter," *Journal of Spacecraft and Rockets*, Vol. 20, No. 1, 1983, pp. 61–69.

[10]Siemers, P., Wolf, H., and Flanagan, P. F., "Shuttle Entry Air Data System Concepts Applied to Space Shuttle Orbiter Flight Pressure Data to Determine Air Data - STS 1-4," *AlAA Aerospace Sciences Meeting, Reno, NV*, No. AIAA 1983-0118, 1983.

[11]Wolf, H., Henry, M. W., and Siemers, P. M., "Shuttle Entry Air Data System (SEADS): Optmization of Preflight Algorithms based on Flight Results," *AIAA Aerodynamic Testing Conference, San Diego, CA*, No. AIAA 1988-2053, 1988.

[12]Whitmore, S., Moes, T., and Larson, T., "Preliminary Results From a Subsonic High Angle-of-Attack Flush Airdata Sensing (HI-FADS) System: Design, Calibration, and Flight Test Evaluation," Tech. Rep. NASA TM 101713, National Aeronautics and Space Administration, 1990.

[13]Anderson, M. B., Lawrence, W. R., and Lopez, J. L., "Supplementing Gradient Search with Genetic Algorithm for Air Data Estimation System," AIAA 1994-1931, *AIAA Applied Aerodynamics Conference, Colorado Springs, CO*, 1994.

[14]Whitmore, A., Moes, R., and Aeronautics, N., "Measurement Uncertainty and Feasibility Study of a Flush Airdata System for a Hypersonic Experiment," Tech. Rep. NASA TM 4627, National Aeronautics and Space Administration, 1994.

[15]Anderson, M. B., Lawrence, W. R., and Lopez, J. L., "Air Data Estimation System for Control of Guided Munitions," AIAA 1993-3458, *AIAA Applied Aerodynamics Conference, Monterey, CA*, 1993.

[16]Anderson, M. B., Lawrence, W. R., and Lopez, J. L., "Air data prediction from surface pressure measurements on guided munitions," *Journal of Guidance, Control, and Dynamics*, Vol. 18, No. 2, 1995, pp. 355–360.

[17]Kasich, D. C. and Cheng, P. Y., "Flush Port / lnertially Blended Air Data Estimator," *AIAA Aerospace Sciences Meeting, Reno, NV*, No. AIAA 1991-0670, 1991.

[18]Deshpande, S., Kumar, R., Seywald, H., and Siemers, P., "Air data system optimization using a genetic algorithm," *AIAA Guidance, Navigation, and Control Conference*, No. AIAA 1992-4466, 1992.

[19]Deb, K., *Multi-Objective Optimization using Evolutionary Algorithms*, John Wiley & Sons, Ltd., 2001.

[20]Padula, S. L., Kincaid, R. K., and William, C., "Optimization Strategies for Sensor and Actuator Placement," Tech. rep., *NASA TM 1999-209126,* National Aeronautics and Space Administration, 1999.

[21]Spencer, D., Blanchard, R., Braun, R., Kallemeyn, P., and Thurman, S., "Mars Pathfinder Entry, Descent, and Landing Reconstruction," *Journal of Spacecraft and Rockets*, Vol. 36, No. 3, 1999, pp. 348–356.

[22]Euler, E., Adams, G., and Hopper, F., "Design and Reconstruction of the Viking Lander Descent Trajectories," *Journal of Guidance, Control, and Dynamics*, Vol. 1, No. 5, 1977, pp. 372–378.

[23]Christian, J., Verges, A., and Braun, R., "Statistical Reconstruction of Mars Entry, Descent, and Landing Trajectories and Atmospheric Profiles," *AIAA SPACE Conference and Exposition*, No. AIAA 2007-6192, 2007.

[24]Wells, G. and Braun, R. D., "Reconstruction of the Spirit Mars Exploration Rover Entry, Descent and Landing Performance," *International ARA Days Conference, Arachon, France*, No. AA 3-2008-16, 2008.

[25]Dutta, S., Clark, I., Russell, R., and Braun, R., "Statistical Entry, Descent, and Landing Performance Reconstruction of the Mars Phoenix Lander," *International Planetary Probe Workshop, Portsmouth, VA*, 2011.

[26]Tapley, B. D., Schutz, B., and Born, G., *Statistical Orbit Determination*, Elsevier Academic Press, Burlington, MA, 2004.

[27]Zarchan, P. and Musoff, H., *Fundamentals of Kalman Filtering, A Practical Approach*, American Institute of Aeronautics and Astronautics, Reston, VA, 2000.

[28]Vinh, N., Busemann, A., and Culp, R., *Hypersonic and Planetary Entry Flight Mechanics*, The University of Michigan Press, Ann Arbor, MI, 1980.

[29]Dutta, S. and Braun, R., "Mars Entry, Descent, and Landing Trajectory and Atmosphere Reconstruction," *AIAA Aerospace Sciences Meeting, Orlando, FL*, No. AIAA 2010-1210, 2010.

[30]Karlgaard, C., Blanchard, R., Kirsch, M., Tartabini, P., and Toniolo, M., "Hyper-X Post-Flight Trajectory Reconstruction," *Journal of Spacecraft and Rockets*, Vol. 43, No. 1, Jan. 2006, pp. 105–115.

[31]Striepe, S., Powell, R., Desai, P., and Queen, E., "Program To Optimize Simulated Trajectories (POST II)," Tech. rep., NASA Internal Document, 2004.

[32]Deb, K., Pratap, A., Agarwal, S., and Meyarivan, T., "A Fast and Elitist Multiobjective Genetic Algorithm: NSGA-II," *IEEE Transactions on Evolutionary Computation*, Vol. 6, No. 2, 2002, pp. 182–197.

[33]Reyes-Sierra, M. and Coello Coello, C. A., "Multi-Objective Particle Swarm Optimizers: A Survey of the State-of-the-Art," *International Journal of Computational Intelligence Research*, Vol. 2, No. 3, 2006, pp. 287–308.

[34]MATLAB, "Software Package, Ver. R2011a," Tech. rep., The MathWorks, Inc., Natick, MA, 2011.